ARCHIVES OF ELECTRICAL ENGINEERING VOL. 74(1), pp. 105–125 (2025)

DOI 10.24425/aee.2025.153015

Super twisting sliding mode controller for multi-functional grid-connected inverter in photovoltaic system

MAHLA DEHGHANI [1], MOHAMMAD MARDANEH [1]✉, MOHAMMAD HOSSEIN SHAFIEI [1], SAEED HASANVAND [2]

[1] *Department of Electrical Engineering, Shiraz University of Technology Shiraz, I.R. Iran*

[2] *Department of Electrical Engineering, Firouzabad Higher Education Center Shiraz University of Technology Shiraz, I.R. Iran*

e-mail: {ma.dehghani/✉ mardaneh/shafiei/s.hasanvand}@sutech.ac.ir

(Received: 10.07.2024, revised: 10.02.2025)

Abstract: In this paper, the performance of a super twisting sliding mode controller (ST-SMC) is investigated for a multifunctional single-stage inverter that connects a photovoltaic (PV) system to the three-phase utility grid supplying the non-linear load. In this work, the single-stage inverter is controlled to improve power quality by compensating the current harmonics of nonlinear load and to inject maximum power from the PV system to the grid with ST-SMC controller. In this way, the ST-SMC controller is implemented to adjust the DC bus voltage to the value determined by the maximum power point tracking (MPPT) algorithm, as well as to the single-stage inverter current control using the synchronous reference frame theory. According to the simulation results, the ST-SMC controller provides high robustness and better performance in transient and steady state conditions. The results show that the total harmonics distortion (THD) of the grid current is reduced to 1.75% and the DC bus voltage reaches its set-point at 0.08 second with a small amount, approximately 0.05%, of the overshoot. In addition, the superiority and accuracy of the proposed scheme is verified by replacing conventional SMC and PI controllers with super twisting sliding mode controllers. Evaluate the suggested scheme's performance is done using the MATLAB/Simulink software.

Key words: harmonic compensation, PV system, single-stage inverter, super-twisting sliding mode control

Abbreviations	
SMC	Sliding mode controller
ST	Super twisting
PV	Photovoltaic
MPPT	Maximum power point tracking
P&O	Perturbation and observation
VSI	Voltage source inverter
MFGTI	Multifunctional grid-tied inverter
SRF	Synchronous reference frame
PCC	Point of common coupling
SPWM	Sinusoidal pulse width modulation
LPF	Low-pass filter
PLL	Phase-locked loop
Nomenclature	
$i_{ind,q}$	Inverter output current in dq frame
$i_{ld,q}$	Load current in dq frame
$S_{d,q}$	Sliding surface in dq frame
$V_{ind,q}$	Inverter output voltage in dq frame
V_g	Utility grid voltage in dq frame
u_{sw}	Super-twisting switching control
$V_{in,eq}$	Equivalent control
$V_{in,\text{ref}}$	Super-twisting sliding mode global law
L_g, R_g	Inductance and resistance of the filter
V_c	DC-bus voltage
i_c	DC-bus capacitor current

1. Introduction

Currently, there are extensive plans to replace fossil energy sources with renewable sources, one of the most important of which is solar energy due to its inexhaustibility. The characteristics of the power production of the photovoltaic (PV) system are affected by various factors, such as solar radiation and the ambient temperature. Hence, the maximum power point tracking (MPPT) algorithm is developed to extract the most power possible from the PV panel in any ambient condition. Various MPPT techniques have been employed [1], such as perturbation and observation (P&O) [2, 3], incremental conductivity (InC) [4, 5], or other artificial intelligence techniques or nonlinear controllers [6, 7]. In this article, P&O technique is utilized for the MPPT algorithm. This method is widely used because of high accuracy in maximum power point (MPP) tracking, easy and simple implementation, requirement minimal computational resources and low cost [8]. Figure 1 shows the flowchart related to the operation of the P&O algorithm.

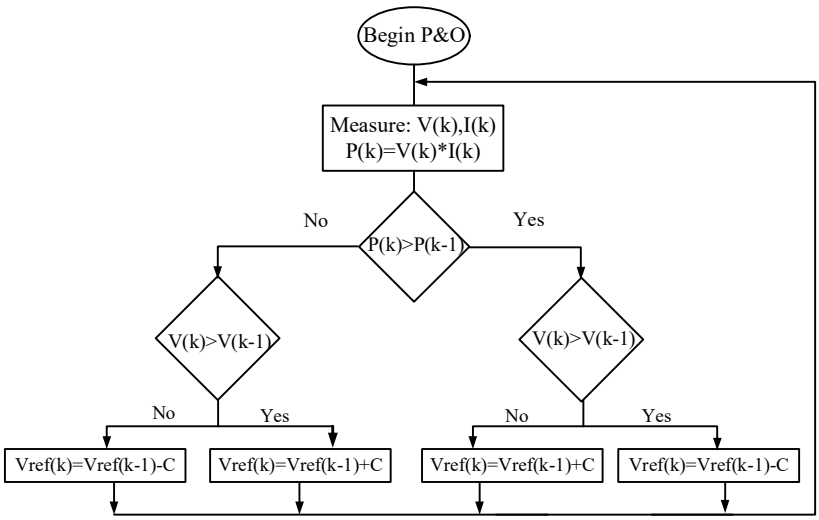

Fig. 1. Flow chart of the P&O algorithm

The vital component for connecting the PV system to the utility grid is a grid-tied inverter. There are two common structures for grid-tied photovoltaic systems: single-stage and two-stage, as shown in Fig. 2 [9, 10].

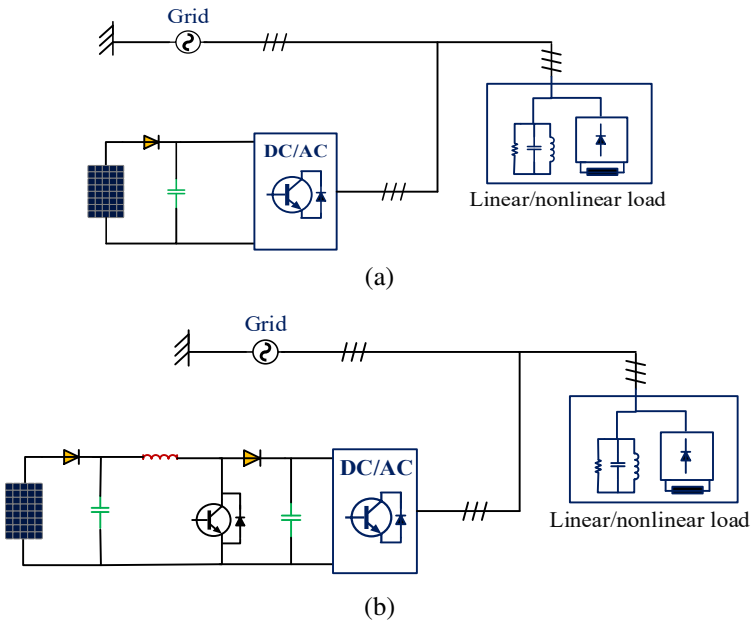

Fig. 2. Various topologies of PV inverter: single-stage structure (a); double-stage structure (b)

In the two-stage architecture, a DC-DC converter amplifies the panel output voltage, and the MPPT algorithm is executed on it. Then, the energy is transferred to the grid by a voltage source inverter (VSI). In the single-stage architecture, PV panels are directly linked to the DC bus of the voltage source inverter. Consequently, by eliminating the DC- DC converter, the single-stage structure has fewer electronic components, higher efficiency, and lower cost compared to the two-stage structure. Moreover, it requires a higher DC voltage level [11, 12]. Nevertheless, the widespread use of the electronic power converters and the non-linear loads leads to harmonic pollution and degrades the power quality of the grid [13]. A multifunctional grid-tied inverter (MFGTI) is reliable solution for compensating the harmonics and improves the power quality. The MFGTI injects active power generated by solar energy in addition to enhancing the power quality of the grid by providing auxiliary services including balancing the load, harmonic reduction and reactive power compensation [14, 15]. In [16], a three-phase multifunctional double-stage inverter with an energy storage system and nonlinear load is utilized. A high-order SMC is developed for compensation of the current harmonic and MPPT optimization. In [15], compensating the nonactive current in addition to active power transfer from the PV system is carried out with a quasi-two-stage multifunctional inverter for PV applications. However, the PI controller is applied to control the inverter current and adjust the DC bus voltage.

In [17], a multifunctional double-stage grid-tied inverter is proposed in the presence a nonlinear load that is controlled by an improved sliding mode control. The output current control is fulfilled using the hysteresis controller, which has the ripple of the current due to switching frequency changes. In [18], several control strategies have been investigated that can reduce the harmonic content in the grid current. Among them, non-linear control approaches are more appropriate for harmonic current tracking and nonlinear systems such as power electronic converters. Among the non-linear control approaches that have been investigated to control grid-tied inverters, sliding mode control (SMC) has some positive features over the other control methods [19, 20]. The sliding mode control has remarkable features due to its robustness to parameter variations and external disturbances, easy and simple implementation, and fast dynamic response. Despite these advantages, the SMC method operates based on the discontinuous control of the sign function, which leads to chattering phenomenon. The chattering phenomenon causes instability, increases losses in power circuits and reduces control accuracy [8, 21]. One of the alternatives to overcome the chattering phenomenon is to use the high-order SMC control technique [18]. The super twisting sliding mode control (ST-SMC) is a higher-order SMC technique [22] that is implemented for diverse applications without requiring additional information. The ST-SMC can reduce chattering in the presence of uncertainty and lead to finite-time convergence to the sliding surface [23–26].

In [27], the ST-SMC controller is employed for the multifunctional double-stage grid-connected photovoltaic system. Meanwhile, the overall efficiency is reduced using a DC-DC converter before the DC-AC converter. In [28], the PV modular is connected to the grid by a three-phase single-stage inverter in nonlinear load conditions, and sliding mode control is utilized to regulate the grid-tied inverter current, despite undesirable chattering phenomenon exists. In [29], sliding mode control is proposed for the control of an active power filter. However, the chattering phenomenon of the SMC controller leads to a loss of accuracy in control. In [30], a super-twisting sliding mode control is developed for current control of a grid-connected inverter in a PV system. Nonetheless, MPPT is not implemented and DC bus voltage has not been controlled.

In this article, a multifunctional three-phase single-stage inverter is utilized to connect the PV system to the grid supplying the nonlinear-load. The section that follows is a description of the article's main contributions:

- The robust super-twisting sliding mode controller – the synchronous reference frame (SRF) theory – P&O algorithm is proposed for the multifunctional grid-tied inverter which is fed by a PV system.
- The super-twisting sliding mode controller has been suggested for the inverter current control and the DC bus voltage adjustment under nonlinear and uncertain conditions.
- The suggested scheme has been presented to eliminate the harmonics of the nonlinear loads using the compensated current of the inverter and the DC bus voltage adjustment based on the set point specified by the MPPT algorithm.
- The performance of the super-twisting sliding mode controller will be compared to the conventional sliding mode controller and PI controller under transient and steady-state conditions.

The paper is organized as following. Section 1 consists of the Introduction. The system configuration and modeling of the main parts is described in Section 2. The inverter current and the DC bus voltage control strategy based on the ST-SMC nonlinear control will be designed and discussed in Section 3. The simulation results of the proposed system are given in Section 4. Finally, the main conclusions are represented in Section 5 .

2. System configuration

Figure 3 indicates the system under study in this article. In this structure, the PV system is connected to the three-phase utility grid using a single-stage inverter. There are three primary parts to the suggested scheme: the harmonic extraction unit, the controller, and the main circuit; In the harmonic extraction section, the current harmonics caused by the non-linear load are extracted and the current references are generated for the controller section. The direct reference harmonic currents components are determined based on the SRF method. The control section generates the control signals according to these references that consists of two main parts: the DC bus voltage adjustment at the value determined by the MPPT algorithm and the current harmonics control system.

The purpose of the current control system is to eliminate the harmonics created by the non-linear load at the point of common coupling (PCC), which is compensated by the injected current of the inverter. In this way, the inverter compensates the reactive power and reduces the harmonics to improve the power quality in addition to injecting the active power from the PV system into the utility grid. Finally, the control signals in the main circuit are developed to activate the inverter switches based on the sinusoidal pulse width modulation (SPWM).

3. System control strategy

The control structure of the system is presented in Fig. 4 which has two main sections. Firstly, the maximum power is extracted from the PV system. Secondly, the nonlinear load harmonics at the PCC are eliminated. In the first part, the maximum power tracking of the PV system is carried

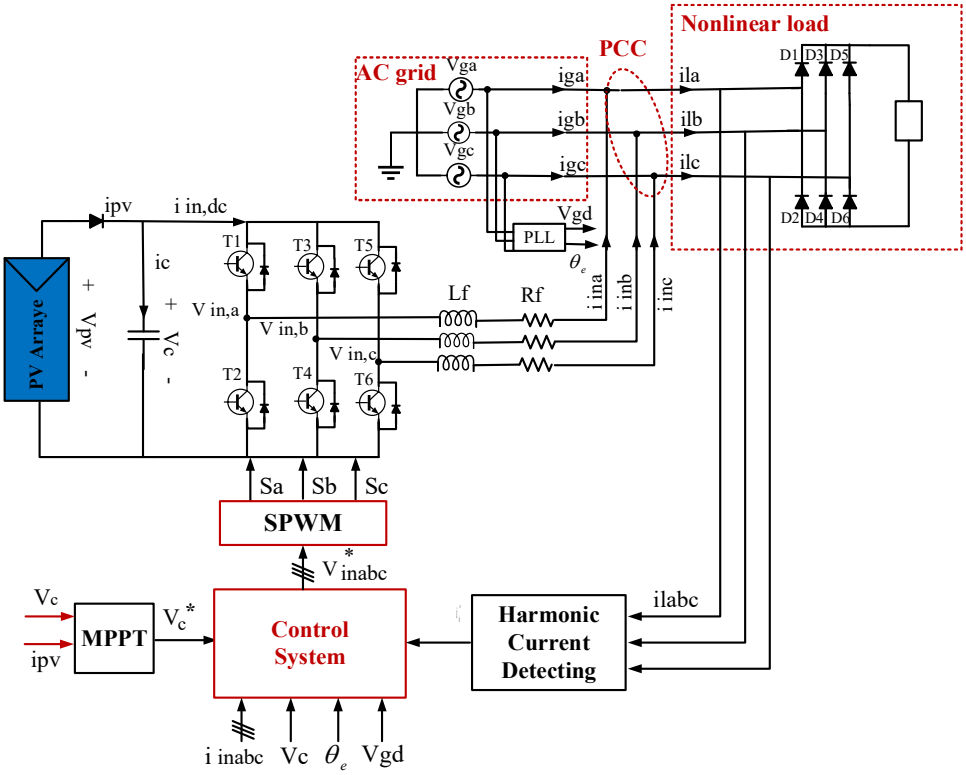

Fig. 3. Overall structure of grid-tied PV system

out by the P&O algorithm and the DC bus voltage is controlled using the ST-SMC control strategy, which creates the reference current corresponding to the active power injected into the utility grid. In the second part, the ST-SMC controller is employed to make the output current of the inverter track the reference current of the inverter. The extraction of low order harmonics of the load is done using a low-pass filter (LPF) that is used to determine the inverter reference current. Thus, the generation of control signals in the *dq*-rotating reference frame is done by processing current control loops through the ST-SMC control strategy, which will be discussed in the next section.

3.1. Inverter current control based on ST-SMC controller

The ST-SMC controller is proposed for keeping the main advantage (robustness) and overcoming the undesired discontinuities in the conventional SMC which has led to the reduction of chattering phenomenon. The main goal of ST-SMC controller is to make $S = \dot{S} = 0$ and it only needs to measure the sliding surface. In this way, the sliding surfaces related to inverter currents control are defined in (1) and (2) forms:

$$S_d = i^*_{ind} - i_{ind}, \tag{1}$$

$$S_q = i^*_{inq} - i_{inq}, \tag{2}$$

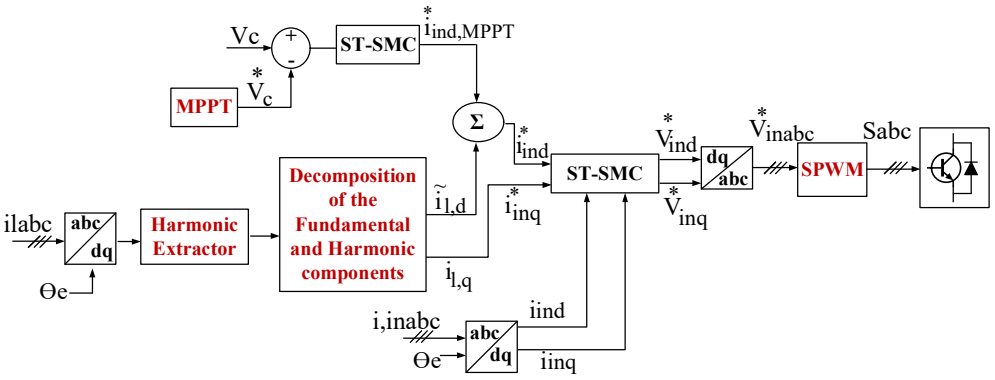

Fig. 4. Control block diagram of the proposed scheme

where $S = [S_d\ S_q]^T$ is the sliding surface, $\boldsymbol{i}^*_{\boldsymbol{in}} = [i^*_{ind}\ i^*_{inq}]^T$ and $\boldsymbol{i}_{\boldsymbol{in}} = [i_{ind}\ i_{inq}]^T$ are the reference current and the inverter output current. The purpose of the current control loop is to force the i_{ind} and i_{inq} currents of the inverter to track the reference currents (i^*_{ind}, i^*_{inq}). The SRF theory is used for the direct harmonic current components. In this way, the measured load current (i_{ld}, i_{lq}) in turn is composed of two parts, an average part denoted by (i^-_{ld}, i^-_{lq}) and an oscillating part caused by harmonics $(i^{\sim}_{ld}, i^{\sim}_{lq})$. The q-axis current of the inverter is responsible to compensate the reactive power and the d-axis current $(i_{ind,\mathrm{MPPT}})$ should be tuned in such a way that the maximum PV available power is injected to the grid. Meanwhile, both d- and q-axis currents have to compensate the load harmonics. Therefore, the reference currents are as (3) and (4):

$$i^*_{in,d} = \widetilde{i}_{ld} + i^*_{ind,\mathrm{MPPT}}, \tag{3}$$

$$i^*_{in,q} = i_{lq}. \tag{4}$$

In ST-SMC, the law control based on a super-twisting algorithm (u_{sw}) is defined by the (5) expression, which is composed of two terms:

$$u_{sw} = u_1 + u_2; \begin{cases} u_1 = -\lambda\,|S|^{\rho}\,\mathrm{sign}\,(S) \\ \dot{u}_2 = -\mu \mathrm{sign}\,(S) \end{cases}, \tag{5}$$

where S is the sliding surface. λ, $\mu$and ρ are the ST-SMC controller gains.

The sufficient conditions for the state trajectory convergence to the sliding surface in finite time are defined by Levant [31] in (6) form:

$$\begin{cases} \lambda^2 \geq \dfrac{4\Phi}{\Gamma_m^2}\dfrac{\Gamma_M(\mu+\phi)}{\Gamma_m(\mu-\phi)} \\ \mu \geq \dfrac{\phi}{\Gamma_m} \\ 0 \leq \rho \leq 0.5 \end{cases}. \tag{6}$$

ϕ is the positive bound of the unknown function h. Γ_M and Γ_m are the upper and lower positive values of unknown function g. The functions h and g belong to $\dfrac{\mathrm{d}^2 S}{\mathrm{d}t^2}$. ρ is a fractional coefficient

which is often fixed at 0.5. For stable operation, the controller gains must be positive constants that the parameters values are tuned by the "trial and error" method. The λ and μ gains are effectives for the response of the system and on steady-state accuracy. Therefore, the switching control (u_{sw}) is simplified by the (7) expression:

$$\begin{aligned} u_{sw} &= \begin{cases} -\lambda\,|S|^{0.5}\,\mathrm{sign}\,(S) + u_2, \\ \dot{u}_2 = -\mu \mathrm{sign}\,(S), \end{cases} \\ u_{sw} &= -\lambda\,|S|^{0.5}\,\mathrm{sign}\,(S) - \mu \int \mathrm{sign}\,(S)\,\mathrm{d}(\tau). \end{aligned} \tag{7}$$

The ST-SMC controller structure is shown in Fig. 5 and the detailed proof of the switching control law will be explained in section 3.3.

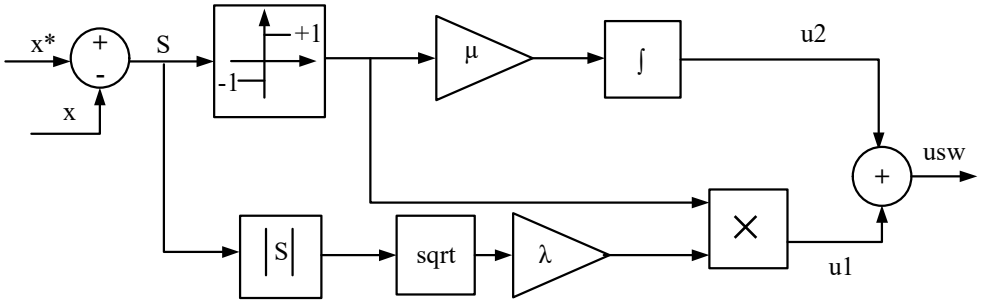

Fig. 5. The ST-SMC controller structure

In this section, the dynamic model of the three-phase, two-level inverter with an L filter in the AC-side according to Kirchhoff's laws is written as (8):

$$L_f \frac{\mathrm{d}i_{in}}{\mathrm{d}t} + R_f i_{in} = V_{in} - V_g, \tag{8}$$

where (9):

$$\begin{aligned} \boldsymbol{i_{in}} &= [i_{ina}\ i_{inb}\ i_{inc}]^T, \\ \boldsymbol{V_{in}} &= [V_{ina}\ V_{inb}\ V_{inc}]^T, \\ \boldsymbol{V_g} &= \left[V_{ga}\ V_{gb}\ V_{gc}\right]^T. \end{aligned} \tag{9}$$

In (9), $\boldsymbol{i_{in}}$, $\boldsymbol{V_{in}}$ and $\boldsymbol{V_g}$ show, respectively, inverter output current, the inverter output voltage, and the utility grid voltage.

For easy controller design, (8) is usually shown in the dq rotating reference frame by the (10) and (11) expressions:

$$\dot{i}_{ind} = \frac{\mathrm{d}i_{ind}}{\mathrm{d}t} = -\frac{R_f}{L_f} i_{ind} + w_e i_{inq} - \frac{V_{gd}}{L_f} + \frac{V_{ind}}{L_f}, \tag{10}$$

$$\dot{i}_{inq} = \frac{\mathrm{d}i_{inq}}{\mathrm{d}t} = -\frac{R_f}{L_f} i_{inq} - w_e i_{ind} - \frac{V_{gq}}{L_f} + \frac{V_{inq}}{L_f}, \tag{11}$$

where (12) and (13):

$$\begin{bmatrix} i_{ind} \\ i_{inq} \end{bmatrix} = \frac{2}{3} T i_{in} \quad \begin{bmatrix} V_{ind} \\ V_{inq} \end{bmatrix} = \frac{2}{3} T V_{in} \quad \begin{bmatrix} V_{gd} \\ V_{gq} \end{bmatrix} = \frac{2}{3} T V_g, \tag{12}$$

$$T = \begin{bmatrix} \cos(wt) & \cos\left(wt - \frac{2\pi}{3}\right) & \cos\left(wt + \frac{2\pi}{3}\right) \\ -\sin(wt) & -\sin\left(wt - \frac{2\pi}{3}\right) & -\sin(wt + \frac{2\pi}{3}) \end{bmatrix}. \tag{13}$$

The frequency and amplitude of the grid are extracted by synchronous reference frame phase-locked loop (SRF-PLL). In (8), L_g and R_g are respectively the inductance and resistance of the filter. The equivalent control terms are obtained by replacing (10) and (11) in the sliding surfaces derivative ((1) and (2)) and equating them to zero, as (14) and (15):

$$V_{ind}^{eq} = L_f \dot{i}_{ind}^{*} + R_f i_{ind} - w_e L_f i_{inq} + V_{gd}, \tag{14}$$

$$V_{inq}^{eq} = L_f \dot{i}_{inq}^{*} + R_f i_{inq} - w_e L_f i_{ind} + V_{gq}. \tag{15}$$

Finally, the global control law of the ST-SMC is given as (16):

$$V_{in,\text{ref}} = u_{sw} + V_{in,eq}. \tag{16}$$

By replacing (7), (14) and (15) in (16), the global control laws for the inverter currents control of the structure proposed are expressed in the (17) and (18) forms:

$$V_{ind}^{*} = R_f i_{ind} - w_e L_f i_{inq} + V_{gd} - \mu_d \sqrt{|S_d|}\text{sign}(S_d) - \lambda_d \int \text{sign}(S_d)\text{d}(\tau), \tag{17}$$

$$V_{inq}^{*} = R_f i_{inq} + w_e L_f i_{ind} + V_{gq} - \mu_d \sqrt{|S_q|}\text{sign}(S_q) - \lambda_q \int \text{sign}(S_q)\text{d}(\tau). \tag{18}$$

3.2. DC-bus voltage control

The DC-bus voltage control is done using ST-SMC controller with the same method. S_{dc} is the sliding surface of the DC- bus voltage by the (19) expression:

$$S_{dc} = V_c - V_c^{*}. \tag{19}$$

The MPPT algorithm determines the DC-bus voltage reference according to the P&O method. According to the mathematical model of the DC-bus capacitor current in (20) and (21):

$$i_c = i_{\text{PV}} - i_{in,\text{DC}}, \tag{20}$$

$$\dot{V}_c = \frac{i_c}{C} = \frac{(i_{\text{PV}} - i_{in,\text{DC}})}{C}. \tag{21}$$

Assuming the ideal inverter, the equation of power balance in DC-AC inverter is defined as (22) and (23):

$$P_{dc} \simeq P_g, \tag{22}$$

$$i_{in\text{DC}} V_c \simeq \frac{3}{2} V_{gd} i_{ind,\text{MPPT}}. \tag{23}$$

The previous equation is placed in the derivative of the sliding surface equation. Consequently, the ST-SMC control law for the DC-bus voltage controller is obtained by the (24) expression:

$$i_{ind,\text{MPPT}}^{*} = \frac{2CV_C}{3V_{gd}} \left(\frac{i_{\text{PV}}}{C} - \mu_{dc} \sqrt{|S_{dc}|}\text{sign}(S_{dc}) - \lambda_{dc} \int \text{sign}(S_{dc})\text{d}(\tau) \right). \tag{24}$$

3.3. Stability proof

The stability analysis is derived by a suitable candidate Lyapunov function as (25) [32]:

$$V_{\text{nom}} = \mu |S| + \frac{1}{2} V^2. \tag{25}$$

The above-dynamic scheme is shown by first-order state-space equation as (26):

$$\dot{x} = ax + bu + \zeta, \tag{26}$$

where x and u represent the state vector and the system input. ξ is the disturbance system which is caused by uncertainties, changing parameters and measurement noises, considering that the system disturbance is limited, is defined by the (27) expression:

$$\xi \leq \xi_{\max} |S|^{0.5} . \tag{27}$$

Therefore, the derivative of the Lyapunov function is given in the (28) form:

$$\dot{V}_{nom} = \mu \text{sign}(S)(-\lambda |S|^{0.5} \text{ sign } (S) + \xi_{\max} |S|^{0.5}). \tag{28}$$

By choosing $\lambda \geq \xi_{\max}$, the system is asymptotically stable since this gradient is negative definite.

4. Discussion and results

In order to verify the performance of the proposed system and its controller during transients and steady-state conditions, the simulations are carried out in MATLAB/Simulink software. Parameters related to the proposed system are given in Table 1.

Table 1. Simulation parameters

Parameters name	Value
R_f (series filter resistance)	0.1 Ω
L_f (series filter inductance)	2 mH
C (DC bus capacitor)	1.5 μF
f_{sw} (switching frequency)	10 kHz
V_{ac} (phase-natural voltage of grid)	120 V
f (system frequency)	60 Hz
V_c (DC bus voltage)	350 V

4.1. Steady-state behavior analysis of the proposed system

Figure 6 and Fig. 7 show, respectively, the grid voltage ($\boldsymbol{V_g}$), the grid current ($\boldsymbol{I_g}$), the load current ($\boldsymbol{I_L}$), and the output current of the inverter ($\boldsymbol{I_{inv}}$) before and after connection of the presented system to the grid. It can be seen that the presented system can provide sinusoidal grid current. Figure 8 demonstrates the total harmonic distortion (THD) of the grid source current before and after compensation. From 0 to 0.2 S, the presented system (the PV system with a grid-tied inverter) is not yet inserted to the grid; therefore, the total non-linear load is supplied by the grid. In this case, the THD of the grid current is equal to 9.5%. After 0.2 S, the proposed system is connected to the PCC, and with harmonics compensation and improvement of power quality, the harmonics level of the grid current is reduced to 1.75% (lower than international standard IEEE 519 2014).

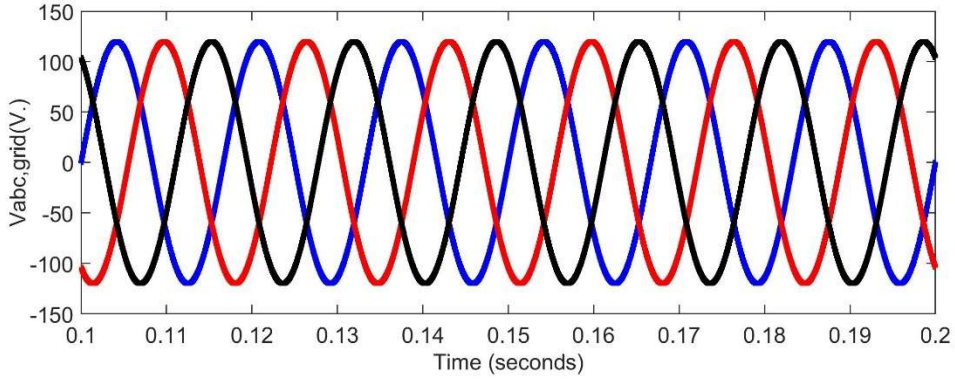

Fig. 6. The grid three-phase voltage before and after the implementation of proposed system

Figure 9 shows the load active power that is equivalent to the sum of the active power of the grid and the average active power produced by PV-VSI. Moreover, the grid power factor is unity and the grid reactive power fluctuates around zero value.

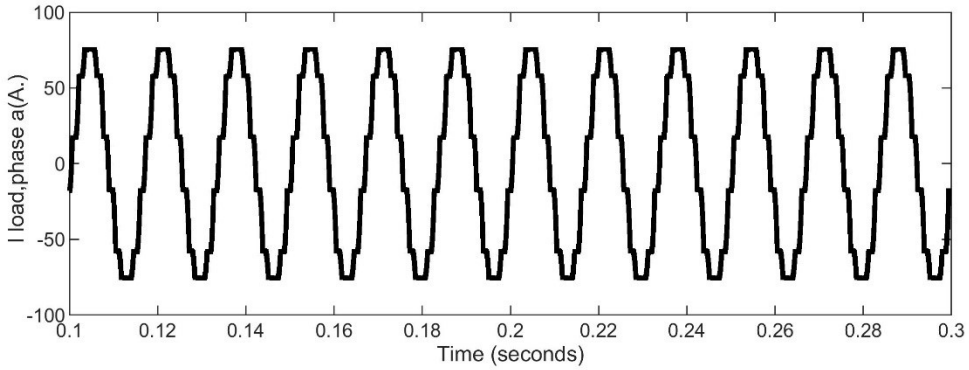

(a)

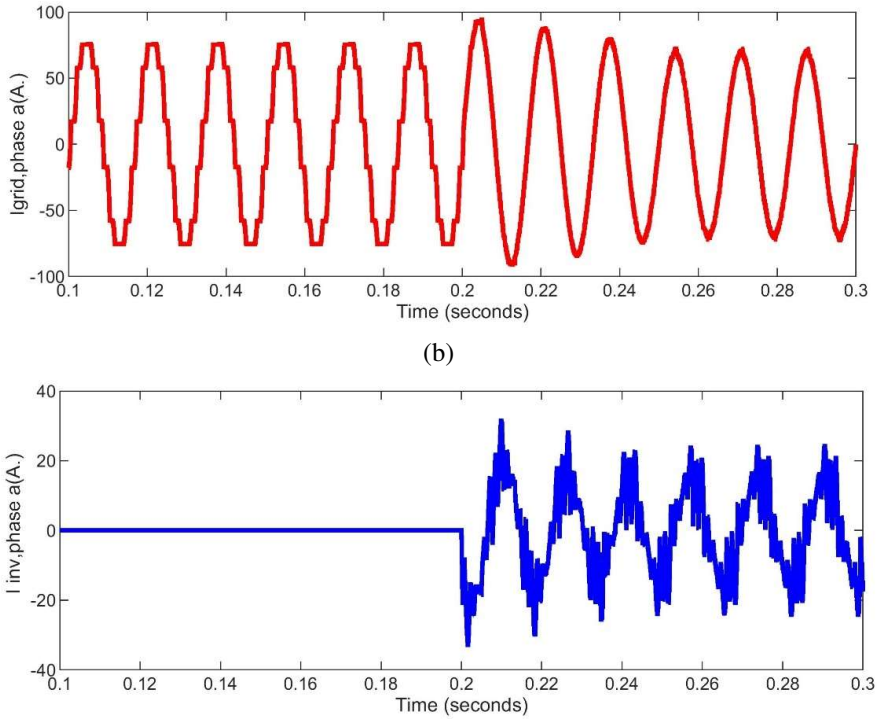

(b)

(c)

Fig. 7. Load current: phase a (a); grid current (b) and inverter current (c). Inverter is suddenly connected to the grid

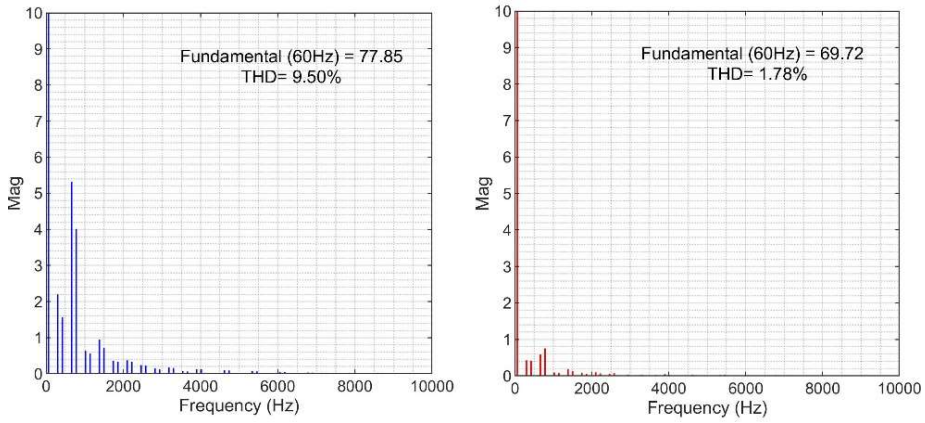

(a) (b)

Fig. 8. Grid current harmonics before (a) and after (b) compensation

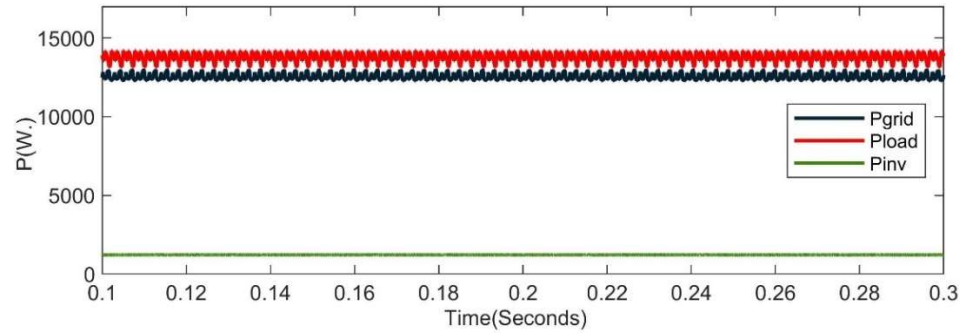

(a)

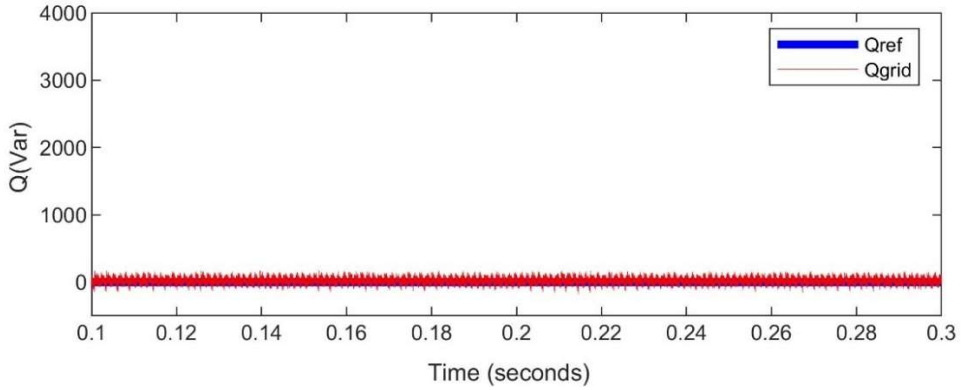

(b)

Fig. 9. The grid active power (a) and the grid reactive power (b)

Figure 10 depicts the ST-SMC controller performance in the DC-bus voltage regulation; it is seen that the desired reference value (350 V) is followed very quickly and without any overshoot.

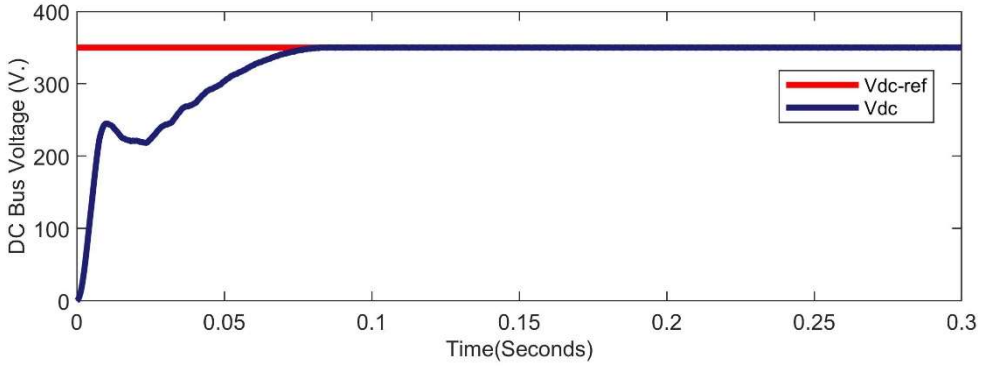

Fig. 10. DC-bus voltage V_{dc}

4.2. Dynamic behavior analysis of the proposed system

In Fig. 11 and Fig. 12 the dynamic performance of the system is assessed in conditions of the sudden load change. The nonlinear load steps at 0.2 s. It can be seen that the grid current is sinusoidal. Moreover, the DC-bus voltage distortion caused by step load change at 0.2 s is regulated rapidly. Hence, the robustness of the proposed system with ST-SMC controller against disturbances is confirmed.

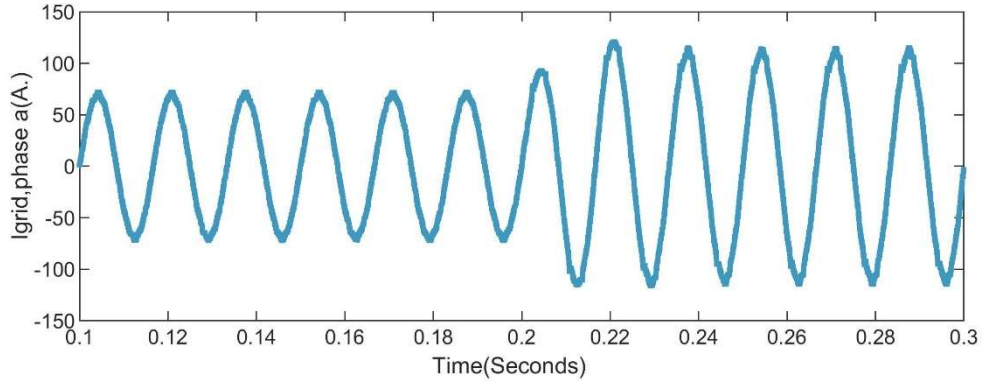

(a)

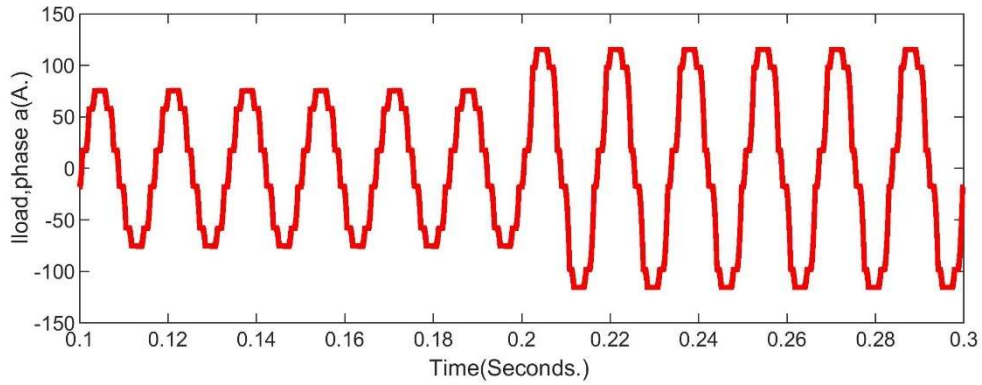

(b)

Fig. 11. Grid current (a) and load current (b) under load change at 0.2 s

In this section, it shows the effectiveness of the proposed system with ST-SMC controller in transient state. Figure 13 demonstrates DC link voltage regulation against irradiance profile changes. It can be seen that the corresponding changes are followed well without any overshoot and fast dynamic response. Therefore, it shows the ability of the proposed system to reject disturbance in DC-link voltage.

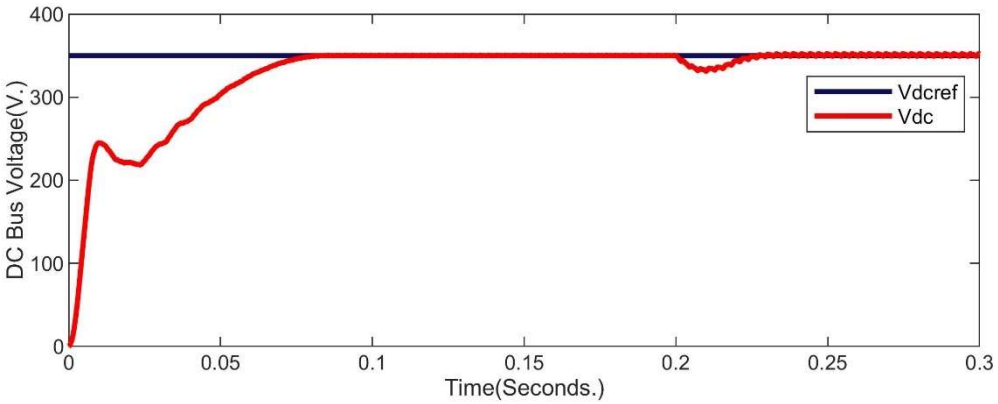

Fig. 12. DC bus voltage under load change at 0.2 s

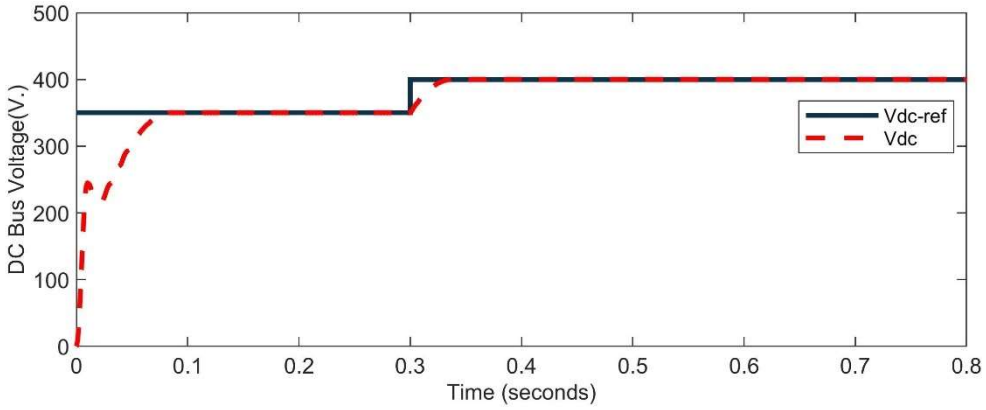

Fig. 13. DC bus voltage response to irradiance level changes

4.3. Comparative analysis

In this section, comparative analyses are carried out between the ST-SMC controller and those of conventional SMC and PI controllers in DC link voltage regulation. Figure 14 shows that the ST-SMC controller performs well without any overshoot and less steady-state error; therefore, it confirms the good stability of the proposed controller.

According to Table 2, the performance of the proposed system using the PI controller and conventional SMC are compared with the ST-SMC controller. In this case, the superiority of the proposed system with the ST-SMC controller in steady state shows that the current harmonic level has improved better and the THD values are below than the IEEE standard (THDi < 5%).

In steady state conditions, the system performance is assessed to ensure smoothness around the reference value using the rip% indicator. In this way, the DC bus voltage ripple (rip) is computed as the difference between the highest and lowest V_{dc} and the average voltage $V_{dc,ave}$ to evaluate

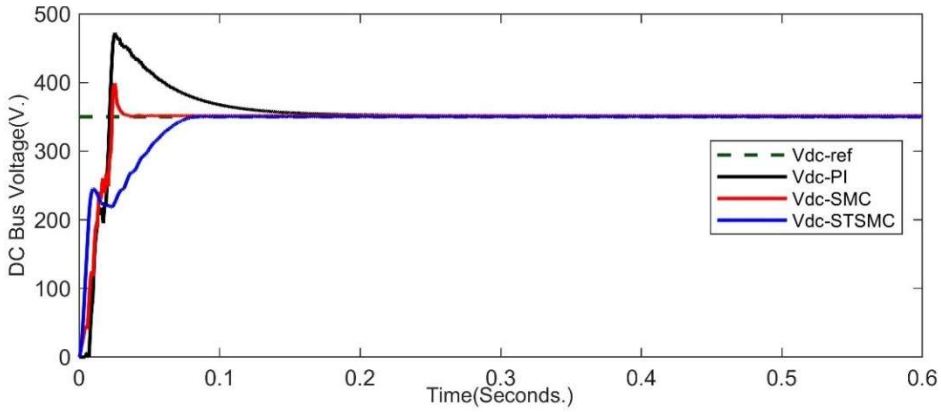

Fig. 14. DC bus voltage with ST-SMC, conventional SMC, and PI controller

the DC bus voltage steady-state error, as (29):

$$\text{rip}\,(\%) = \frac{(V_{dc,\max} - V_{dc,\min})}{V_{dc,ave}} \times 100. \tag{29}$$

The integral absolute error (IAE) indicator is defined to investigate the absolute surface to track the reference of the DC bus voltage in (30) form:

$$\text{IAE} = \int |e(t)|\,\mathrm{d}t. \tag{30}$$

Table 2. Comparing the performance of the ST-SMC with conventional SMC and PI controller

Performances	PI	Conventional SMC	ST-SMC
THD of grid current before filtering (%)	9.5%	9.5%	9.5%
THD of grid current after filtering (%)	2.84%	2.78%	1.75%
DC bus voltage settling time (S.)	0.22	0.06	0.08
DC bus voltage overshoot (%)	34.45%	14.93%	0.05%
rip (%)	0.97%	0.22%	0.034%
IAE	10.36	6.78	5.02

The conventional SMC suffers from the chattering phenomenon, which causes high-order harmonics in the output current. Hence, ST-SMC has been used to overcome this problem. In Fig. 15, according to the fast Fourier transform (FFT) analysis, the high-order harmonics are reduced in the ST-SMC controller.

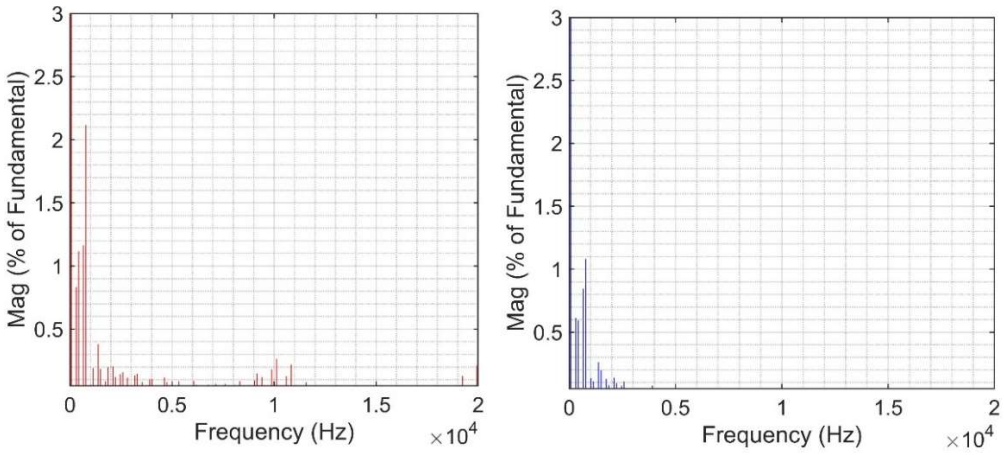

(a) (b)

Fig. 15. Comparing the spectra of the grid current in conventional SMC (a) and ST-SMC (b)

4.4. Grid distortion analysis

In Fig. 16 and Fig. 17, the proposed system performance is evaluated in the condition of the imbalanced grid voltage and the presence of the nonlinear load. It is shown that the presented system is able to decrease the harmonic of the grid in the presence of the imbalance voltage of the grid.

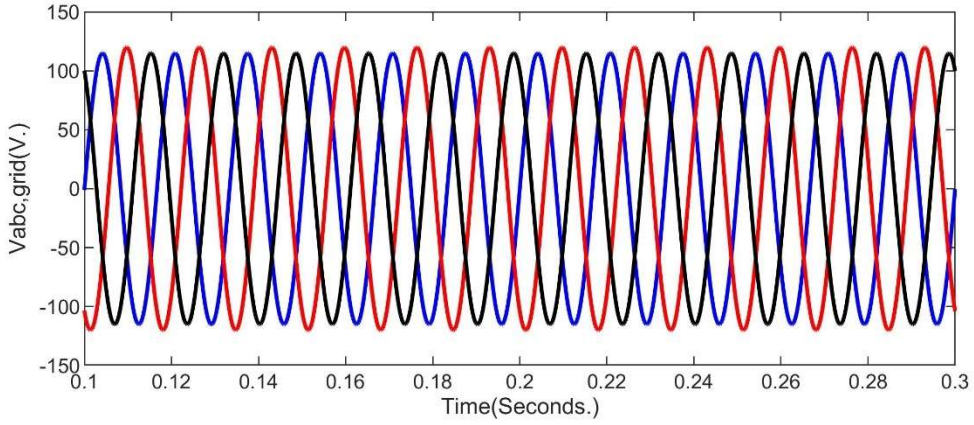

Fig. 16. Voltage of the three-phase grid under unbalanced grid voltage

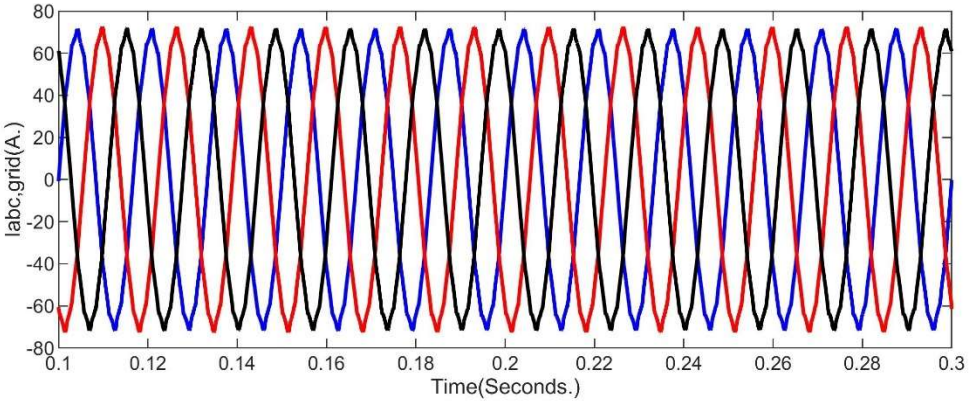

(a)

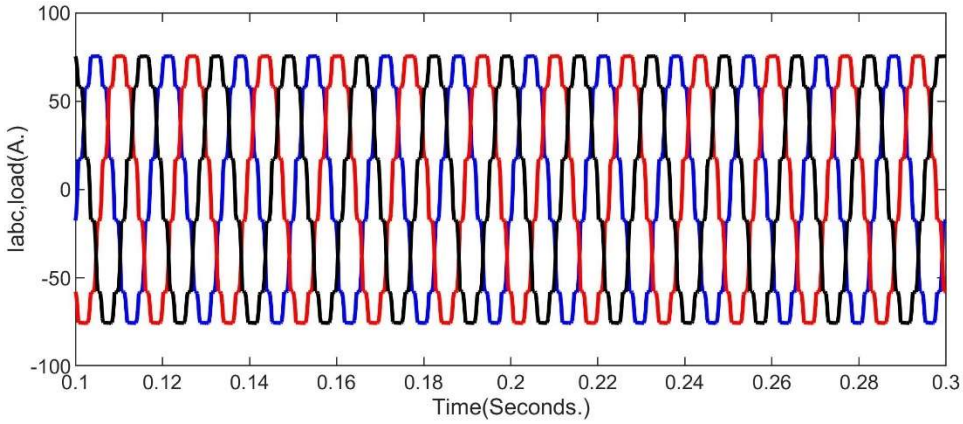

(b)

Fig. 17. The three-phase grid current (a) and the load current (b) under unbalanced grid voltage

5. Conclusions

In this paper, the modeling and control of the grid-tied inverter that connects the PV panels to the utility grid under non-linear load has been discussed. The design of the control loops of the inverter has been done using the ST-SMC robust controller for regulating the DC link voltage to the determined reference value using the MPPT algorithm as well as eliminating the current harmonics created by the non-linear load, which improves the power quality of the grid. The simulation results have demonstrated satisfactory performance that the proposed system with the ST-SMC controller is attained a lower THD level 1.75% and the DC link voltage can track the reference value well with a settling time about of 0.08 s and almost without overshoot. In this way, the effective results in dynamic and steady state response confirm the effectiveness of the ST-SMC control method compared to conventional SMC and PI control methods. On the other hand, the simulation results confirm the stability and robustness of the system against any external disturbances under various conditions of solar radiation and non-linear load changes. In the future,

a suitable and effective structure for grid-connected inverter configuration can be applied to reduce harmonics and improve power quality based on topology structure and modulation scheme. In addition, a suitable current control techniques and advanced MPPT algorithms is recommended to improve the MFGTI's performance under normal and abnormal Conditions.

References

[1] Kabalcı E., *Review on novel single-phase grid-connected solar inverters: Circuits and control methods*, Solar Energy, vol. 198, pp. 247–274 (2020), DOI: 10.1016/j.solener.2020.01.063.

[2] Manoharan P. *et al*., *Improved perturb and observation maximum power point tracking technique for solar photovoltaic power generation systems*, IEEE Systems Journal, vol. 15, no. 2, pp. 3024–3035 (2020), DOI: 10.1109/JSYST.2020.3003255.

[3] Abdel-Salam M., El-Mohandes M.T., Goda M., *An improved perturb-and-observe based MPPT method for PV systems under varying irradiation levels*, Solar Energy, vol. 171, pp. 547–561 (2018), DOI: 10.1016/j.solener.2018.06.080.

[4] Shang L., Guo H., Zhu W., *An improved MPPT control strategy based on incremental conductance algorithm*, Protection and Control of Modern Power Systems, vol. 5, no. 2, pp. 1–8 (2020), DOI: 10.1186/s41601-020-00161-z.

[5] Singh P., Shukla N., Gaur P., *Modified variable step incremental-conductance MPPT technique for photovoltaic system*, International Journal of Information Technology, vol. 13, pp. 2483–2490 (2021), DOI: 10.1007/s41870-020-00450-8.

[6] Harrison A., Alombah N.H., de Dieu Nguimfack Ndongmo J., *A New Hybrid MPPT Based on Incremental Conductance-Integral Backstepping Controller Applied to a PV System under Fast-Changing Operating Conditions*, International Journal of Photoenergy, vol. 2023, no. 1, 9931481 (2023), DOI: 10.1155/2023/9931481.

[7] Ali M.N., Mahmoud K., Lehtonen M., Darwish M.M., *An efficient fuzzy-logic based variable-step incremental conductance MPPT method for grid-connected PV systems*, IEEE Access, vol. 9, pp. 26420–26430 (2021), DOI: 10.1109/ACCESS.2021.3058052.

[8] Mahmod Mohammad A.N., Mohd Radzi M.A., Azis N., Shafie S., Atiqi Mohd Zainuri M.A., *An enhanced adaptive perturb and observe technique for efficient maximum power point tracking under partial shading conditions*, Applied Sciences, vol. 10, no. 11, 3912 (2020), DOI: 10.3390/app10113912.

[9] Guo B., *Optimization design and control of single-stage single-phase PV inverters for MPPT improvement*, IEEE Transactions on Power Electronics, vol. 35, no. 12, pp. 13000–13016 (2020), DOI: 10.1109/TPEL.2020.2990923.

[10] Vairavasundaram I., Varadarajan V., Pavankumar P.J., Kanagavel R.K., Ravi L., Vairavasundaram S., *A review on small power rating PV inverter topologies and smart PV inverters*, Electronics, vol. 10, no. 11, 129 (2021), DOI: 10.3390/electronics10111296.

[11] Kolantla D., Mikkili S., Pendem S.R., Desai A.A., *Critical review on various inverter topologies for PV system architectures*, IET Renewable Power Generation, vol. 14, no. 17, pp. 3418–3438 (2020), DOI: 10.1049/iet-rpg.2020.0317.

[12] Sahoo S.K., Sukchai S., Yanine F.F., *Review and comparative study of single-stage inverters for a PV system*, Renewable and Sustainable Energy Reviews, vol. 91, pp. 962–986 (2018), DOI: 10.1016/j.rser.2018.04.063.

[13] Elallali A., Abouloifa A., Lachkar I., Taghzaoui C., Giri F., Mchaouar Y., *Nonlinear control of grid-connected PV systems using active power filter with three-phase three-level NPC inverter*, IFAC-PapersOnLine, vol. 55, no. 12, pp. 61–66 (2022), DOI: 10.1016/j.ifacol.2022.07.289.

[14] Daravath R., Sandepudi S.R., *Control of multifunctional inverter to improve power quality in grid-tied solar photo voltaic systems*, International Journal of Emerging Electric Power Systems, vol. 24, no. 6, pp. 743–754 (2023), DOI: 10.1515/ijeeps-2022-0117.

[15] Wang J., Sun K., Wu H., Zhang L., Zhu J., Xing Y., *Quasi-two-stage multifunctional photovoltaic inverter with power quality control and enhanced conversion efficiency*, IEEE Transactions on Power Electronics, vol. 35, no. 7, pp. 7073–7085 (2019), DOI: 10.1109/TPEL.2019.2956940.

[16] Naamane D., Laid Z., Fateh M., *Power quality improvement based on third-order sliding mode direct power control of microgrid-connected photovoltaic system with battery storage and nonlinear load*, Iranian Journal of Science and Technology, Transactions of Electrical Engineering, vol. 47, no. 4, pp. 1473–1490 (2023), DOI: 10.1007/s40998-023-00627-4.

[17] Safa A., Berkouk E.M., Messlem Y., Gouichiche A., *A robust control algorithm for a multifunctional grid tied inverter to enhance the power quality of a microgrid under unbalanced conditions*, International Journal of Electrical Power & Energy Systems, vol. 100, pp. 253–264 (2018), DOI: 10.1016/j.ijepes.2018.02.042.

[18] Dehkordi N.M., Sadati N., Hamzeh M., *A robust backstepping high-order sliding mode control strategy for grid-connected DG units with harmonic/interharmonic current compensation capability*, IEEE Transactions on Sustainable Energy, vol. 8, no. 2, pp. 561–572 (2016), DOI: 10.1109/TSTE.2016.2611383.

[19] Utkin V.I., *Sliding mode control design principles and applications to electric drives*, IEEE Transactions on Industrial Electronics, vol. 40, no. 1, pp. 23–36 (1993), DOI: 10.1109/41.184818.

[20] Komurcugil H., Biricik S., Bayhan S., Zhang Z., *Sliding mode control: Overview of its applications in power converter*s, IEEE Industrial Electronics Magazine, vol. 15, no. 1, pp. 40–49 (2020), DOI: 10.1109/MIE.2020.2986165.

[21] Utkin V., Lee H., *Chattering problem in sliding mode control systems*, in International Workshop on Variable Structure Systems, VSS'06, IEEE, pp. 346–350 (2006), DOI: 10.1016/j.arcontrol.2007.08.001.

[22] Levant A., *Sliding order and sliding accuracy in sliding mode control*, International Journal of Control, vol. 58, no. 6, pp. 1247–1263 (1993), DOI: 10.1080/00207179308923053.

[23] Ze K. *et al.*, *Design of super twisting sliding mode controller for a three-phase grid-connected photovoltaic system under normal and abnormal conditions*, Energies, vol. 13, no. 15, 3773 (2020), DOI: 10.3390/en13153773.

[24] Lu J., Savaghebi M., Ghias A.M., Hou X., Guerrero J.M., *A reduced-order generalized proportional integral observer-based resonant super-twisting sliding mode control for grid-connected power converters*, IEEE Transactions on Industrial Electronics, vol. 68, no. 7, pp. 5897–5908 (2020), DOI: 10.1109/TIE.2020.2998745.

[25] Gonzalez T., Moreno J.A., Fridman L., *Variable gain super-twisting sliding mode control*, IEEE Transactions on Automatic Control, vol. 57, no. 8, pp. 2100–2105 (2011), DOI: 10.1109/TAC.2011.2179878.

[26] Shen X. *et al.*, *High-performance second-order sliding mode control for NPC converters*, IEEE Transactions on Industrial Informatics, vol. 16, no. 8, pp. 5345–5356 (2019), DOI: 10.1109/TII.2019.2960550.

[27] Deffaf B., Hamoudi F., Debdouche N., Amor Y.A., Medjmadj S., *Super-twisting Sliding Mode Control for a Multifunctional Double Stage Grid-connected Phoovoltaic System*, Advances in Electrical and Electronic Engineering, vol. 20, no. 3, 240 (2022), DOI: 10.15598/aeee.v20i3.4454.

[28] Dehghani M., Mardaneh M., Shafiei M.H., *Sliding mode control for load harmonics compensation and PV voltage regulation in a grid-tied inverter through a single-stage MPPT*, in 2020 IEEE 28th Iranian Conference on Electrical Engineering (ICEE), Tabriz, Iran, pp. 1–6 (2020), DOI: 10.1109/ICEE50131.2020.9260854.

[29] Cortajarena J.A., Barambones O., Alkorta P., Cortajarena J., *Sliding mode control of an active power filter with photovoltaic maximum power tracking*, International Journal of Electrical Power & Energy Systems, vol. 110, pp. 747–758 (2019), DOI: 10.1016/j.ijepes.2019.03.070.

[30] Del Pizzo A., Di Noia L.P., Meo S., *Super twisting sliding mode control of smart-inverters grid-connected for PV applications*, in 2017 IEEE 6th International Conference on Renewable Energy Research and Applications (ICRERA), pp. 793–796 (2017), DOI: 10.1109/ICRERA.2017.8191168.

[31] Levant A., *Higher-order sliding modes, differentiation and output-feedback control*, International Journal of Control, vol. 76, no. 9–10, pp. 924–941 (2003), DOI: 10.1080/0020717031000099029.

[32] Barth A., Reichhartinger M., Reger J., Horn M., Wulff K., *Lyapunov-design for a super-twisting sliding-mode controller using the certainty-equivalence principle*, IFAC-PapersOnLine, vol. 48, no. 11, pp. 860–865 (2015), DOI: 10.1016/j.ifacol.2015.09.298.